

Supporting Information

Ligand-Mediated Bifunctional Catalysis for the Enhanced Oxygen Reduction and Methanol Oxidation Tolerance in Fuel Cells

Linfang Lu,^{†a} Zhiqiang Wang,^{†b} Shihui Zou,^{†a} Yuheng Zhou,^a Wei Hong,^a Renhong Li,^c Liping Xiao,^a Juanjuan Liu,^d Xue-Qing Gong^{*b} and Jie Fan^{*a}

^aKey Lab of Applied Chemistry of Zhejiang Province, Department of Chemistry, Zhejiang University, Hangzhou 310027, China. *E-mail: xueshan199@163.com; jfan@zju.edu.cn

^bKey Laboratory for Advanced Materials, Centre for Computational Chemistry and Research Institute of Industrial Catalysis, School of Chemistry and Molecular Engineering, East China University of Science and Technology, Shanghai 200237, China. *E-mail: xgong@ecust.edu.cn

^cKey Lab of Advanced Textile Materials and Manufacturing Technology, Ministry of Education of China, Zhejiang Sci-Teck University, Hangzhou 310027, China.

^dCollege of Materials & Environmental Engineering, Hangzhou Dianzi University, Hangzhou 310036, China.

[†]These authors contributed equally to this work.

Detailed experimental procedures

1. Materials.

Commercial Pt/C (20 wt% of Pt, Pt nanoparticles: 3.0 nm) catalyst, Nafion (5%) and triphenylphosphine (>99%) were purchased from Alfa Aesar. Chloroplatinic acid hexahydrate ($\text{H}_2\text{PtCl}_6 \cdot 6\text{H}_2\text{O}$), methanol (CH_3OH , 99.99%), pyridine (99.99%), 4-dimethylaminopyridine (99.99%), butylamine (99.99%), perchloric acid (HClO_4 , 99.99%) and potassium hydroxide (KOH, 99.99%) were purchased from Sinopharm Chemical Reagent Corporation. Oleylamine (80%-90%) were purchased from Aladdin Industrial Corporation. All chemicals were used as received.

2. Electrochemical measurements.

All the electrochemical measurements were carried out on an electrochemical workstation (CH Instruments, Inc., Model CHI 750E) at room temperature ($\sim 25^\circ\text{C}$), using a three-electrode electrochemical system equipped with a rotating disk electrode (RDE) (RRDE, Japan). The cell consisted of a glassy carbon working electrode (3 mm diameter, 0.071 cm^2), a carbon rod counter electrode, and a saturated calomel electrode (SCE). The SCE was isolated by a double reference electrode to ensure the stability of SCE in acid or alkaline medium. The potential versus SCE was transferred to that versus RHE using the following equation: $E(\text{V})$ versus RHE = $E(\text{V})$ versus SCE + $0.059 \times \text{pH} (\text{V}) + 0.2438\text{ V}$.

To prepare catalyst-modified working electrodes, Pt/C catalyst was dispersed in a mixture of water/2-propanol/Nafion (v/v/v = 4/1/0.025) under sonication to form a 4 mg mL^{-1} catalyst ink (totally 1 mL). $\sim 3\ \mu\text{L}$ of this ink was dropped onto the surface of the GC electrode (the actual Pt loadings on electrode were controlled at $15\ \mu\text{g}_{\text{Pt}}\text{ cm}^{-2}$), and then dried under the ambient condition.

The cyclic voltammogram (CV) experiments were conducted in a N_2 or O_2 -saturated 0.1 M HClO_4 or 0.1 M KOH solution with a scan rate of 50 mV s^{-1} . The linear sweep voltammograms (LSVs) were obtained in the O_2 -saturated 0.1 M HClO_4 or 0.1 M KOH solution at rotation speeds of 1600 rpm and with a scan rate of 10 mV s^{-1} . The kinetic current was calculated based on the following equations¹⁻²:

$$\frac{1}{J} = \frac{1}{J_L} + \frac{1}{J_K} = \frac{1}{B\omega^{1/2}} + \frac{1}{J_K} \quad (1)$$

$$B = 0.62nFC_0(D_0)^{2/3}\nu^{-1/6} \quad (2)$$

Where J is the measured current density (mA cm^{-2}), J_L and J_K are the diffusion- and kinetic-limiting current densities (mA cm^{-2}). B is the Levich slope which is given by (2). n is the number of electron transferred for the ORR. ω is the rotation speed in rpm. F is the faraday constant (96485 C mol^{-1}). ν is the kinetic viscosity ($0.01\text{ cm}^2\text{ s}^{-1}$) and D_0 is the diffusion coefficient of O_2 in 0.1 M HClO_4 or 0.1 M KOH ($1.9 \times 10^{-5}\text{ cm}^2\text{ s}^{-1}$). The bulk concentration of oxygen C_0 is $1.2 \times 10^{-6}\text{ mol cm}^{-3}$.

CV profiles were recorded at a sweep rate of 50 or 10 mV s^{-1} , and in a potential window between 0.03 and 1.24 V versus RHE. The MOR was conducted in a N_2 -saturated 0.1 M HClO_4 + 0.1 M CH_3OH or 0.1 M KOH + 0.1 M CH_3OH solution. For CH_3OH crossover test, a calculated portion of CH_3OH was directly added into the aqueous solution with O_2 bubbling. For CO stripping, pure CO was bubbled through

the electrolyte for 15 min while holding the working electrode at 0.05 V versus RHE. Then, Ar was bubbled for another 15 min to remove excess CO from the solution before CO stripping was performed. The electrochemical active surface areas (ECSAs) were calculated by integrating the Coulombic charge for hydrogen desorption or CO stripping in the cyclic voltammeteries (CVs) recorded in N₂-saturated 0.1 M HClO₄ or 0.1 M KOH aqueous solution.

For ECSAs obtained from hydrogen desorption³⁻⁵:

$$ECSA_H = \frac{Q_H}{0.21[Pt]} \quad (3)$$

where Q_H (mC) is the charge due to the hydrogen desorption in the hydrogen region (0.05–0.45 V) of the CVs, 0.21 mC cm⁻² is the electrical charge associated with monolayer adsorption of hydrogen on Pt, and [Pt] is the loading of Pt on the working electrode.

For ECSAs obtained from CO stripping³⁻⁶:

$$ECSA_{CO} = \frac{Q_{CO}}{0.42[Pt]} \quad (4)$$

where Q_{CO} (mC) is the charge due to the CO desorption in the CO adsorbed region (0.8–1.1 V) of the CVs, 0.42 mC cm⁻² is the electrical charge associated with monolayer adsorption of CO on Pt, and [Pt] is the loading of Pt on the working electrode.

3. Pt/C catalyst with different surface coverages of ligands.

The working electrode modified with Pt/C catalyst was firstly activated in O₂-saturated electrolyte solution for 20 cycles to clean the surface of Pt NPs. The process will be discussed in detail in our recent paper published elsewhere. After then, the working electrode was washed by deionized water for three times and immersed in pyridine solution with different concentrations (0.2, 0.5, 1 and 10 μM) for 30 s followed by removing the residual pyridine by deionized water for three times. The electrocatalytic performance was then performed. The schematic illustration was demonstrated in Scheme S1. To the modification of other ligands, the pyridine aqueous solution was changed to oleylamine-ethanol mixture, butylamine-ethanol mixture, dimethylaminopyridine-aqueous solution or triphenylphosphine-ethanol mixture.

4. The preparation of 1wt.% Pt/SiO₂ catalyst.

Pt/SiO₂ (1wt.%) catalyst was prepared by a conventional impregnation method.⁷ Briefly, 1 g of H₂PtCl₆·6H₂O was dissolved in 100 mL of deionized water. Subsequently, 5.3 mL of above solution and 200 mg of silica microsphere were added into a beaker (100 mL). After stirring at a temperature of 80 °C for 2 h, the solid product was obtained and grinded after the water was evaporated. The 1% Pt/SiO₂ catalyst was obtained followed by reducing the above solid product at a temperature of 300 °C in a tube furnace for 1 h under a mixed hydrogen (5%)/argon atmosphere.

5. The denotation of surface coverage of ligand.

The surface coverage of ligand on Pt NPs was calculated based on the decreased electrochemical surface area of Pt, which was calculated from hydrogen desorption or CO stripping:

$$\theta_{s,H} = \frac{\text{total Pt surface area} - \text{exposed Pt surface area}}{\text{total Pt surface area}}$$

$$= \frac{S_{H\text{-fresh}} - S_{H-X}}{S_{H\text{-fresh}}} \quad (5)$$

Where $S_{H\text{-fresh}}$ is the surface area of surface cleaned Pt calculated from hydrogen desorption, S_{H-X} is the surface area of Pt after immersed in X μM pyridine solution for 30 s.

$$\theta_{S,\text{CO}} = \frac{\text{total Pt surface area} - \text{exposed Pt surface area}}{\text{total Pt surface area}} \\ = \frac{S_{\text{CO-fresh}} - S_{\text{CO-X}}}{S_{\text{CO-fresh}}} \quad (6)$$

Where $S_{\text{CO-fresh}}$ is the surface area of surface cleaned Pt calculated from CO stripping, $S_{\text{CO-X}}$ is the surface area of Pt after immersed in X μM pyridine solution for 30 s.

6. Physical characterization.

X-ray photoelectron spectrum (XPS) was measured on an VG Scientific ESCALAB Mark II spectrometer using a monochromatic Al $K\alpha$ X-ray source (1486.6 eV) with a 500 μm spot and an anode power of 150 W. All XPS spectra were corrected using the C 1s line at 284.7 eV. The X-ray powder diffraction (XRD) patterns were recorded on an X-ray diffractometer (Rigaku Ultima IV) with Cu $K\alpha$ radiation operated at a tube voltage of 40 kV and current of 40 mA in the range 10–80°. Transmission electron microscopy (TEM) images were recorded on a Hitachi HT-7700 electron microscope. High-resolution TEM (HRTEM) images were obtained on a JEOL JEM-2100F. The actual Pt loadings on electrode in this work were determined by inductively coupled plasma mass spectrometry (ICP-MS), which were carried out in Agilent 7700 using the diluted solution containing calculated Pt/C in aqua regia.

In situ diffuse reflectance infrared Fourier transform spectroscopy (DRIFTS) was gathered with a Nicolet IS50 spectrometer equipped with a mercury cadmium telluride (MCT) detector at a resolution of 4 cm^{-1} using 32 scans. For Pt/SiO₂ sample, Pt/SiO₂ catalyst was put in a furnace and reduced *in situ* with 20% H₂/Ar at 300 °C for 1 h, followed by cooling to room temperature. The background spectrum was then recorded. After that, 1% CO/Ar was introduced into the sample for 30 min, and the spectra were collected till the steady state. Then pure Ar was introduced to the sample to remove the extra CO gas, and the spectra of chemisorbed CO species were collected. For Pt/SiO₂-py sample, Pt/SiO₂ catalyst was reduced *in situ* with 20% H₂/Ar at 300 °C for 1 h, followed by cooling to room temperature. Then pyridine was adsorbed onto the sample using Ar-blow method (pure pyridine solution) followed by 1% CO/Ar was introduced into the sample. The following procedure was the same as described above.

7. DFT calculations.

Density functional theory (DFT) calculations were carried out using the Vienna Ab-initio Simulation Package (VASP)⁸. The spin-polarized projector augmented wave (PAW) method⁹ and the Perdew-Burke-Ernzerhof (PBE)¹⁰ electron exchange-correlation functional of the generalized gradient approximation (GGA)¹¹ were applied in our calculations. The kinetic energy cut-off for the wave function expanded in the plane-wave basis was set as 400 eV. To optimize the structures, the calculation was performed until the maximum force upon each relaxed atom was less than 0.05 eV \AA^{-1} . The vacuum height was set as 12 \AA to eliminate the interaction between

neighboring slabs. The spin-polarized calculations were carried out with the DFT (PBE) - D3 (BJ) scheme^{12, 13} as implemented in VASP. Default values of the dispersion coefficient (C_6) and the vdW radii (R_0) parameters given by Grimme^{12, 13} were employed.

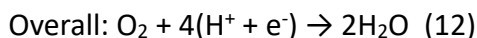
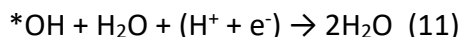
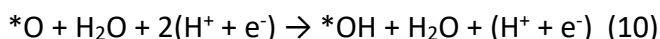
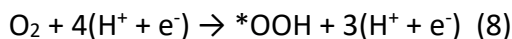
The adsorption energy (E_{ads}) was calculated as follows:

$$E_{\text{ads}} = E_{\text{substrate}} + E_{\text{gas-phase adsorbate}} - E_{\text{total}} \quad (7)$$

where E_{total} is the calculated total energy of the adsorption system, $E_{\text{substrate}}$ is the energy of the clean substrate and $E_{\text{gas-phase adsorbate}}$ is the energy of the gas-phase molecule (include carbon monoxide, oxygen, methanol and pyridine).

In order to study the adsorption of carbon monoxide, methanol or oxygen with different coverage of pyridine on platinum surfaces, we used the models that a 5×5 surface cell was used to construct a five-layer Pt(111) slab, and the top three layers of the Pt(111) slab were allowed to relax. The Brillouin-zone integration was performed along with a 2×2×1 Monkhorst-Pack grid for the {111} surface slabs.

The four-electron ORR mechanisms were investigated on the different coverage of pyridine on Pt nanoparticles in the present work. In acid medium each ORR step can be summarized as follows,

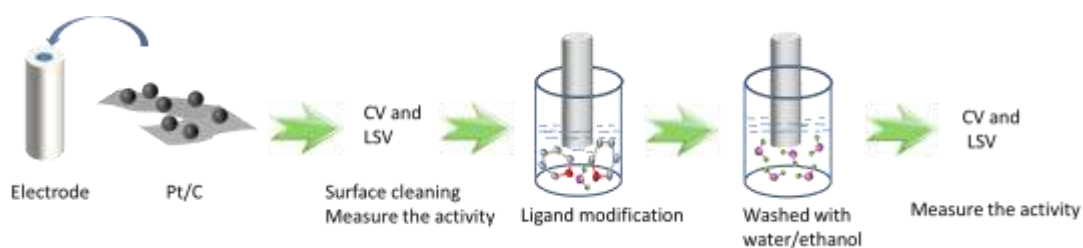


The free energy diagrams of the oxygen reduction reactions (ORR) have been calculated according to the method developed by Nørskov *et al.*¹⁴ Free energy change from initial states to final states of the reaction is calculated as follows:

$$\Delta G = \Delta E + \Delta ZPE - T\Delta S + \Delta G_U + G_{\text{pH}} + \Delta G_{\text{field}} \quad (13)$$

where ΔE is the total energy change obtained from DFT calculations, ΔZPE is the change in zero-point energy, T is the temperature (298.15 K), and ΔS is the change in entropy. $\Delta G_U = eU$, where U is the electrode potential with respect to standard hydrogen electrode, and e is the charge transferred. $\Delta G_{\text{pH}} = k_B T \ln 10 \times \text{pH}$, where k_B is the Boltzmann constant, and $\text{pH}=0$ for acid medium in this study^{15, 16}. ΔG_{field} is the free energy correction due to the electrochemical double layer and is neglected as in previous studies^{14, 16}. Gas-phase H_2O at 0.035bar was used as the reference state, because at this pressure gas-phase H_2O is in equilibrium with liquid water at 298.15 K. The free energy of O_2 was obtained from the free energy change of the reaction $\text{O}_2 + 2\text{H}_2 \rightarrow 2\text{H}_2\text{O}$, which is -4.92 eV at 298.15 K and a pressure of 0.035bar¹⁴. The free energy of $(\text{H}^+ + \text{e}^-)$ in solution at standard conditions of $U=0$ and $\text{pH}=0$ is equal to that of $1/2 \text{H}_2$ according to a computational hydrogen electrode model suggested by Nørskov *et al.*¹⁴, whereas at finite potential and $\text{pH}=0$, it is shifted by $-eU$, as used in some previous studies¹⁴⁻¹⁷. The free energy of OH^- was calculated from the reaction $\text{H}^+ + \text{OH}^- \rightarrow \text{H}_2\text{O}$, which is in equilibrium in water solution¹⁵. The entropies and vibrational frequencies of the species in gas phase were taken from the NIST database¹⁸. Zero-point energy and entropies of the adsorbed species were calculated from the vibrational frequencies. The DFT total energies, ZPE, TS, and Gibbs free energies of

gas molecules were taken from the reference reported¹⁹. Based on those data, we can calculate the free energy change ΔG of each step for the ORR on catalytic surfaces.



Scheme S1. Schematic illustration of the modification of ligand on carbon supported Pt nanoparticles.

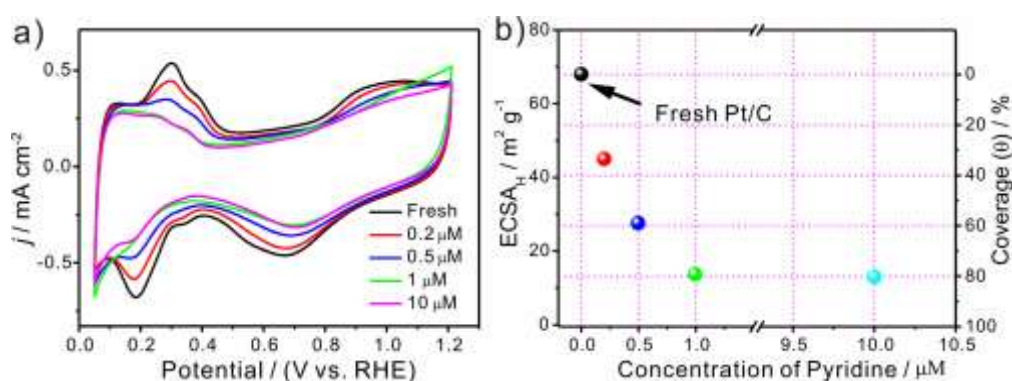


Fig. S1 (a) CVs operated in N₂-saturated 0.1 M KOH solution of Pt/C catalyst before and after immersed in different concentrations of pyridine solution. (b) The variation of electrochemical surface area derived from hydrogen desorption (ECSA_H) and surface coverage (θ) of ligand as a function of pyridine concentration.

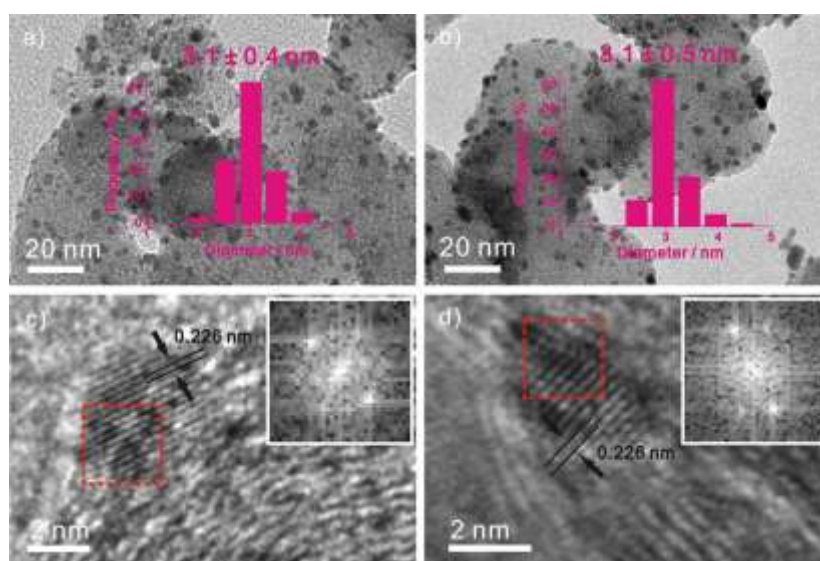


Fig. S2 TEM images of Pt/C before (a) and after (b) modification of pyridine. HRTEM images of Pt/C before (c) and after (d) modification of pyridine. The insets on top right corner of (c) and (d) are the FFT patterns of lattice fringes marked in red dotted square.

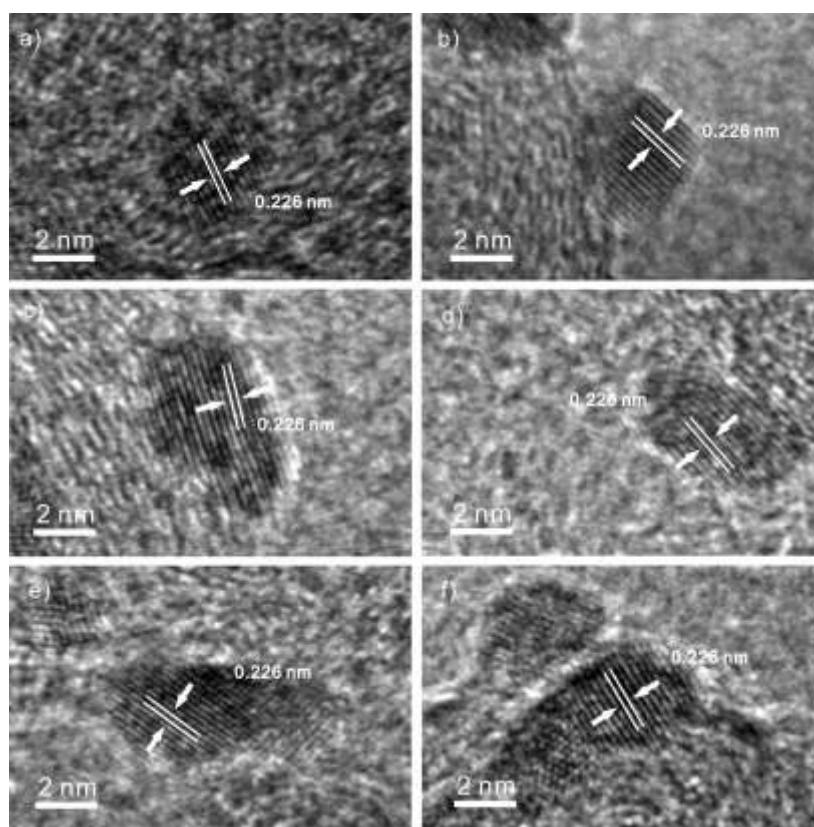


Fig. S3 HRTEM images of Pt nanoparticles before (a, c, e) and after (b, d, f) adsorption of pyridine.

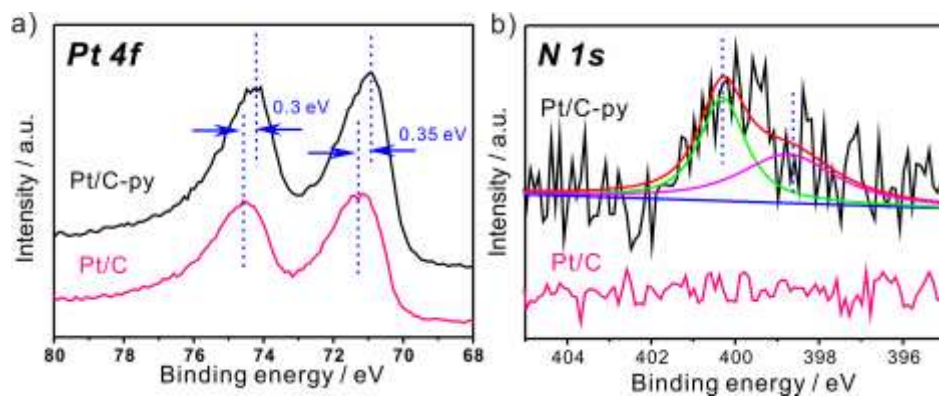


Fig. S4 XPS results of Pt 4f (a) and N 1s (b) of Pt/C and pyridine modified Pt/C (Pt/C-py).

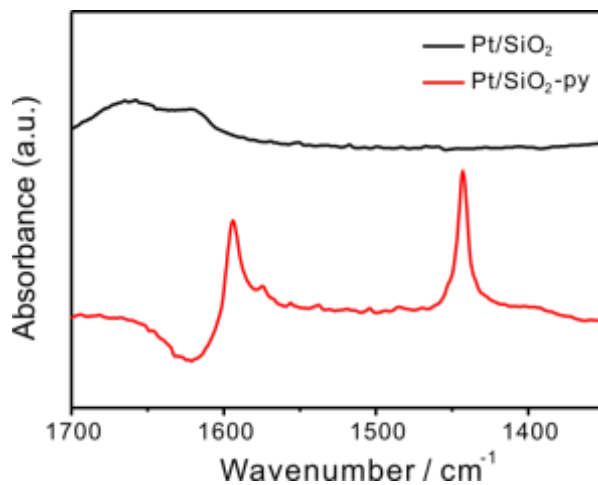


Fig. S5 Fourier transform infrared spectroscopy (FTIR) of Pt/SiO₂ and pyridine modified Pt/SiO₂ (Pt/SiO₂-py).

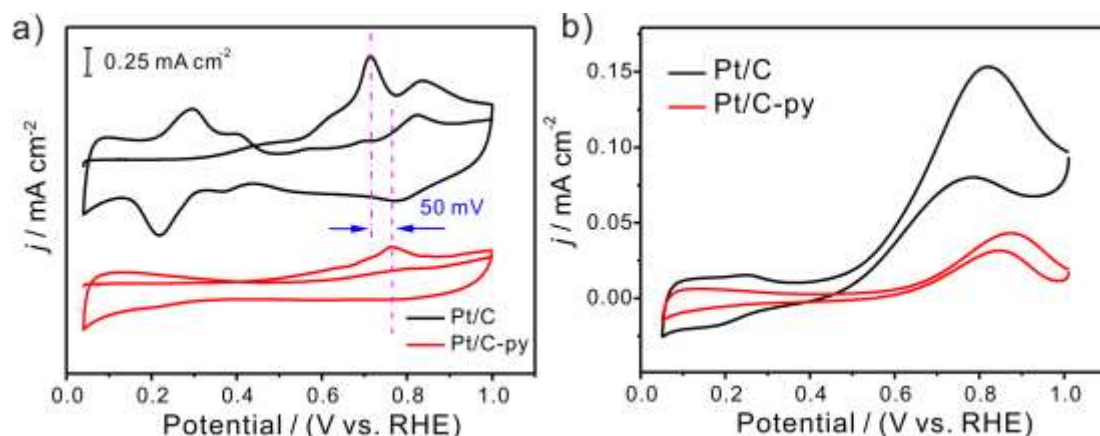


Fig. S6 (a) CO stripping curves in 0.1 M KOH of Pt/C, Pt/C modified with saturated pyridine ligand (Pt/C-py). (b) MOR curves in 0.1 M KOH + 0.1 M CH₃OH solution of Pt/C and Pt/C-py.

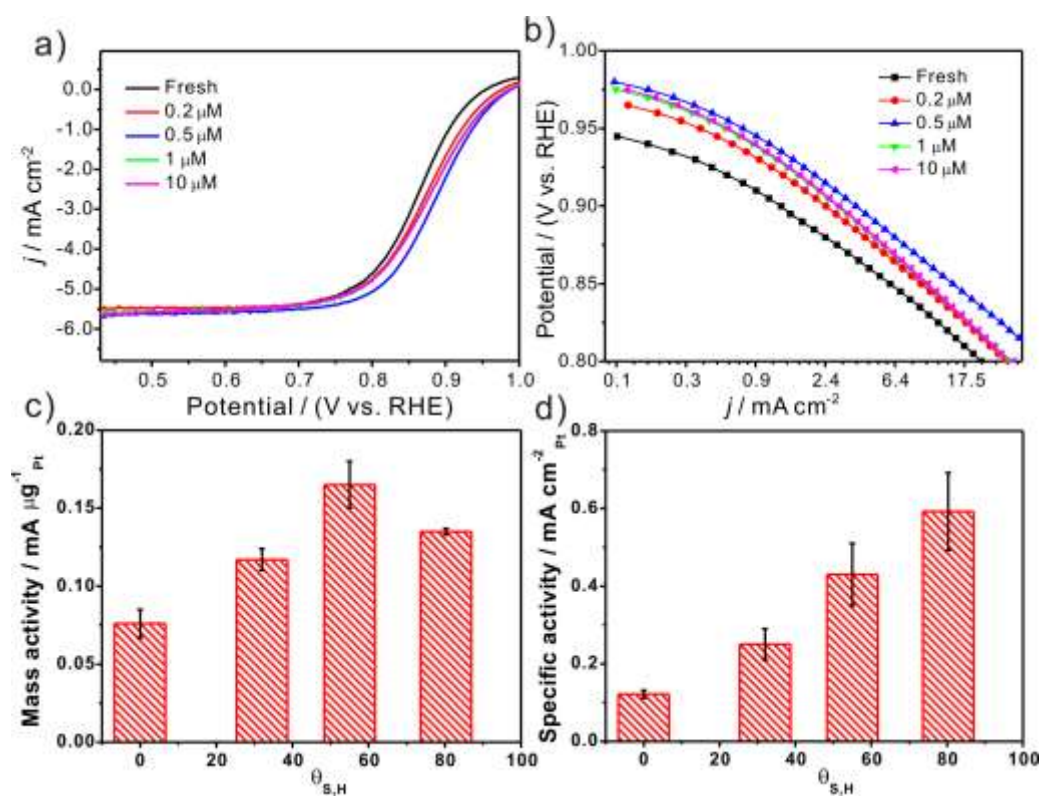


Fig. S7 (a) ORR activity in 0.1 M KOH solution of Pt/C catalyst before and after immersed in different concentrations of pyridine solution. (b) The relationship between potential and kinetic current density of Pt/C catalyst before and after immersed in different concentrations of pyridine solution. ORR mass activity (c) and specific activity (d) in 0.1 M KOH at 0.9 V of Pt/C catalysts with different surface coverages of pyridine derived from hydrogen desorption ($\theta_{S,H}$).

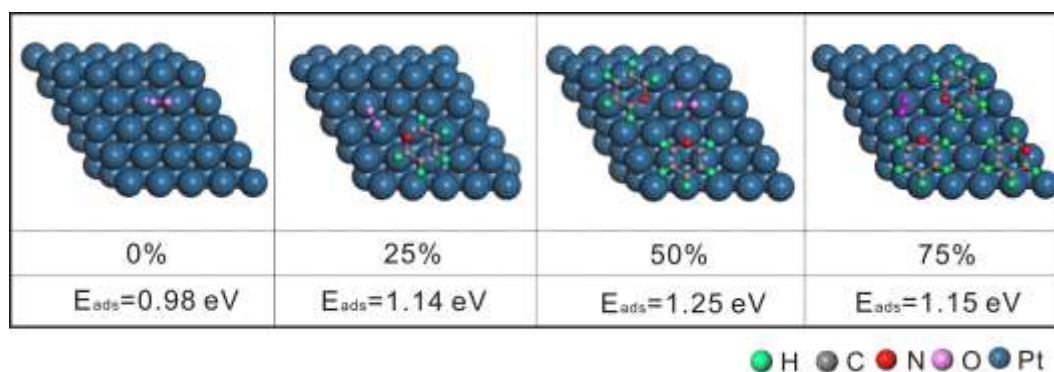


Fig. S8 The adsorption model and energy of O_2 on Pt(111) of pre-adsorbed pyridine with a coverage of 0, 25, 50 and 75%.

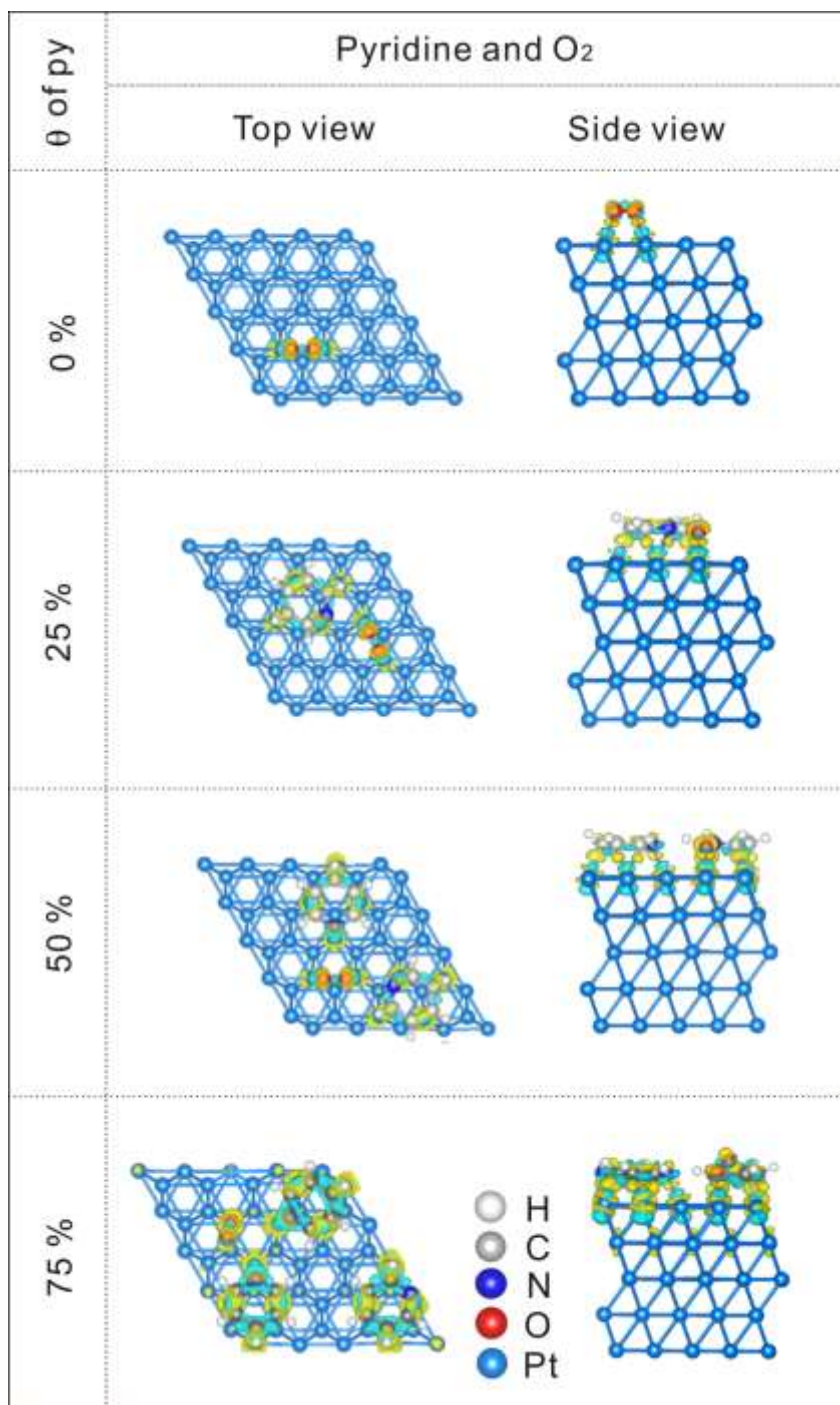


Fig. S9 The Bader charge analysis of O₂ on Pt(111) with different coverages of pyridine.

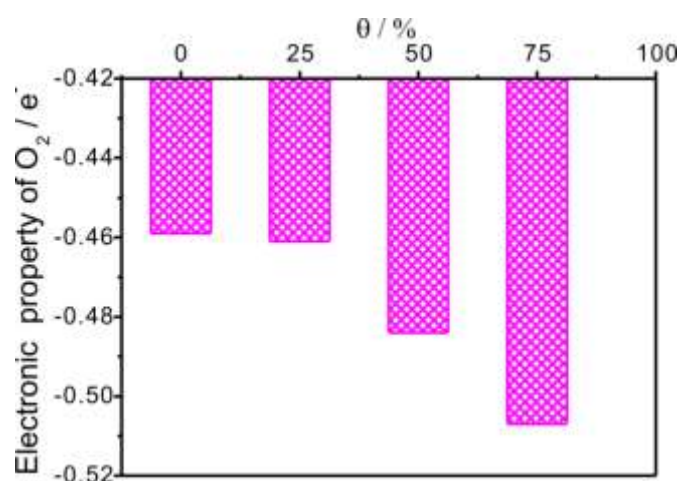


Fig. S10 Electronic property of O₂ on Pt(111) with different coverages of pyridine.

Table S1. Adsorption energy of CO on Pt(111) with different coverages of pyridine.

Coverage of py	0	25%	50%	75%
CO _{ad}	2.12 eV	2.19 eV	2.33 eV	2.48 eV

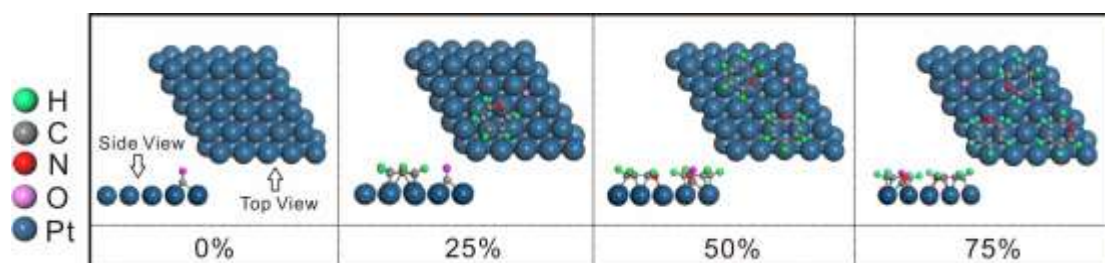


Fig. S11 Calculated adsorption structures of CO at Pt(111) with pre-adsorbed pyridine under the coverages of 0%, 25%, 50% and 75%.

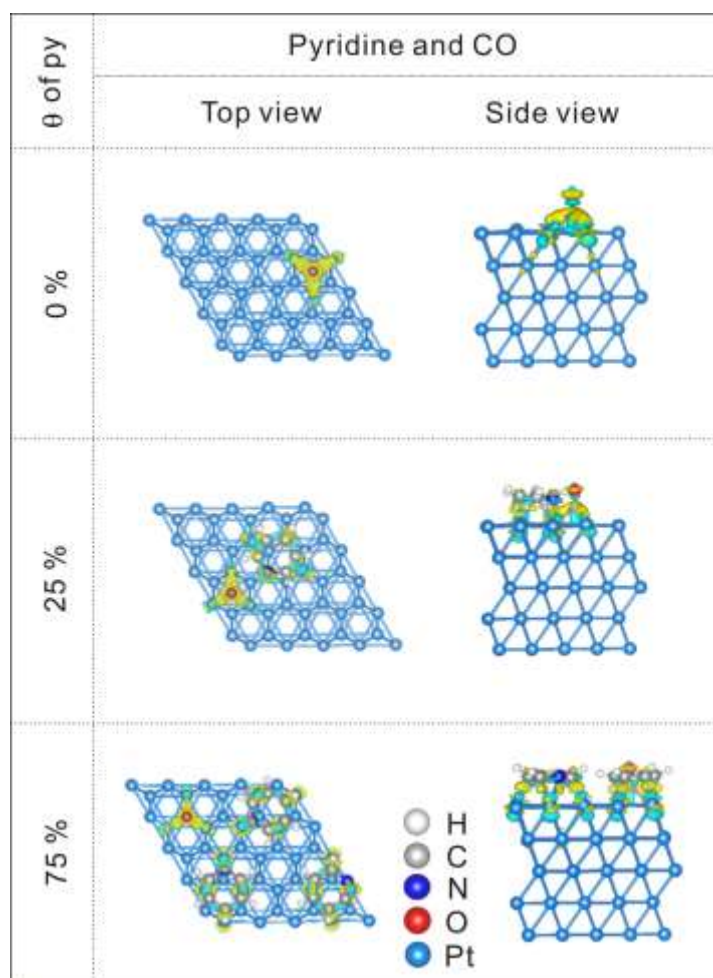


Fig. S12 The Bader charge analysis of CO on Pt(111) with different coverages of pyridine.

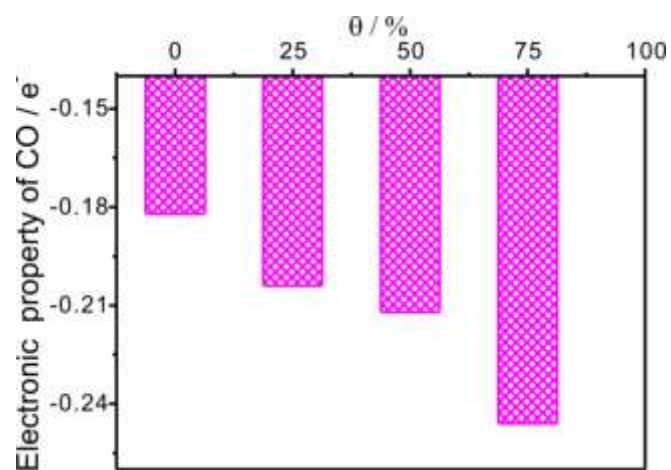
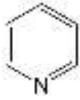


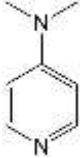
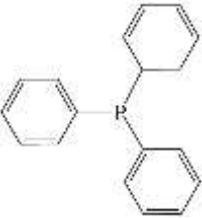


Fig. S13 Electronic property of CO on Pt(111) with different coverages of pyridine.

Table S2 Physicochemical properties of the organic ligands

Ligands	Abbreviation	Structure
Pyridine	Py	
Oleylamine	OAm	
Butylamine	BAm	
4-dimethylaminopyridine	DMAP	
Triphenylphosphine	TPP	

The reasons why above ligands were selected:

Based on the experimental and theoretical analysis, it was found that the electronic effect of ligand was important to obtain the bifunctional catalyst in ORR and MOR. To further investigate the electronic effect on the catalytic performance, it is crucial to compare the ligands with different electron donating abilities. Here, OAm is chosen as an alkylamine ligand whose electron donating ability is weaker than that of pyridine. Besides, considering that OAm is a commonly used ligand in colloidal synthesis, the study of impact of OAm on catalytic activity is also important in heterogeneous catalysis. Observing that the electronic effect of OAm is not as strong as that of pyridine in ORR and MOR, we further used shorter carbon-chain of alkylamine (butylamine) to demonstrate that the alkylamine indeed had less electronic effect than pyridine. On the other hand, considering that the substituent group in 4-dimethylaminopyridine (DMAP) can further donate electrons to the pyridine ring, DMAP was selected as a ligand whose electron donating ability is stronger than that of pyridine. Similar to pyridine, DMAP exhibits both electronic and steric effects. At given surface coverage, Pt/C modified by DMAP even shows slightly higher ORR activity than Pt/C-py. The above results led us to think if the electronic effect came from the pyridine ring (similar as benzene ring). Considering that TPP has more benzene rings and it was often used as an electron-donating ligand in homogeneous catalysis, we thus determined its effects in ORR and MOR and found it had both of the electronic and steric effects.

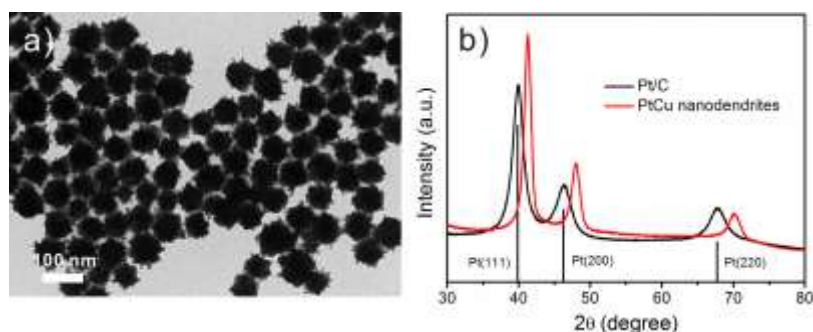


Fig. S14 TEM image (a) and XRD pattern (b) of as-synthesized PtCu alloy nanodendrites (NDs). (c) XPS spectra of PtCu NDs and pyridine modified PtCu NDs (PtCu NDs-py).

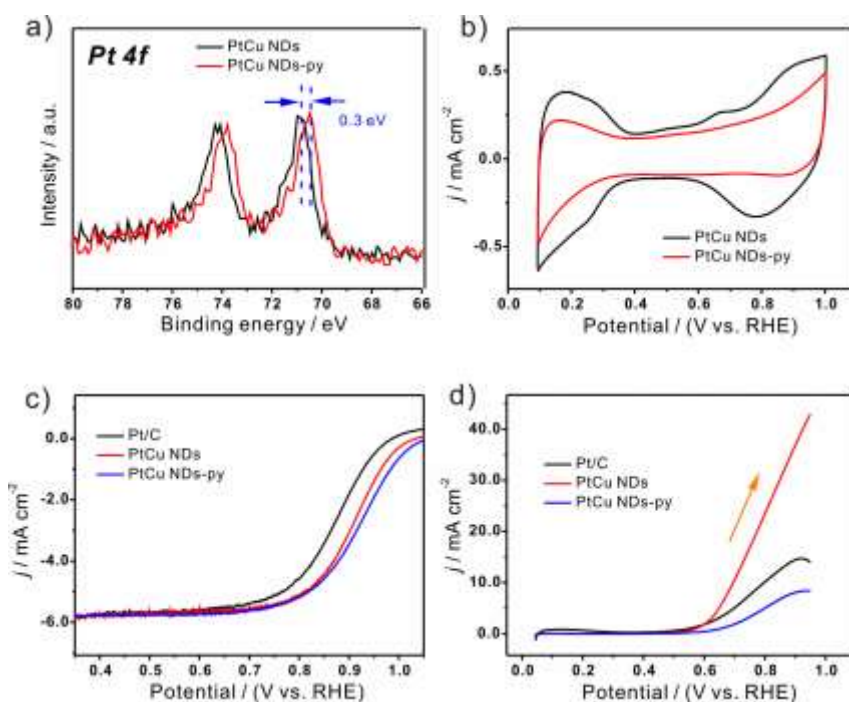


Fig. S15 (a) XPS Pt 4f spectra of PtCu nanodendrites (NDs) and pyridine-saturated PtCu NDs (PtCu NDs-py). (b) CVs of PtCu NDs and PtCu NDs-py operated in N_2 -saturated 0.1 M $HClO_4$. (c) ORR LSV curves of Pt/C, PtCu NDs and PtCu NDs-py in O_2 -saturated 0.1 M $HClO_4$. (d) MOR LSV curves of Pt/C, PtCu NDs and PtCu NDs-py in N_2 -saturated 0.1 M $HClO_4$ + 0.1 M CH_3OH solution.

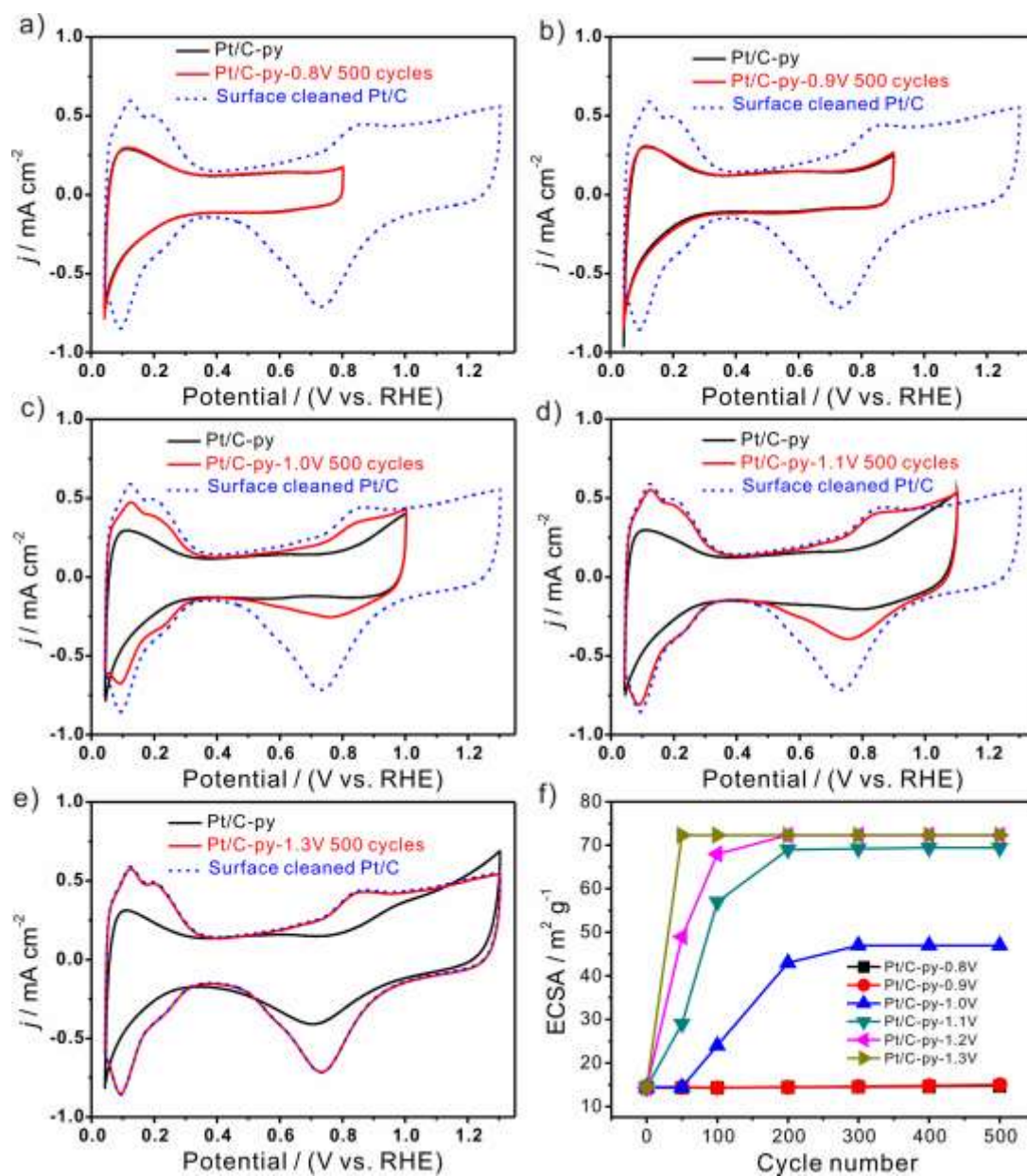


Fig. S16 CV curves of Pt/C-py before and after 500 cycles from 0.05 V to a specific potential. (a) 0.8 V, (b) 0.9 V, (c) 1.0 V, (d) 1.1 V, (e) 1.3 V. (f) The variation of ECSA after different cycles from 0.05 V to a specific potential.

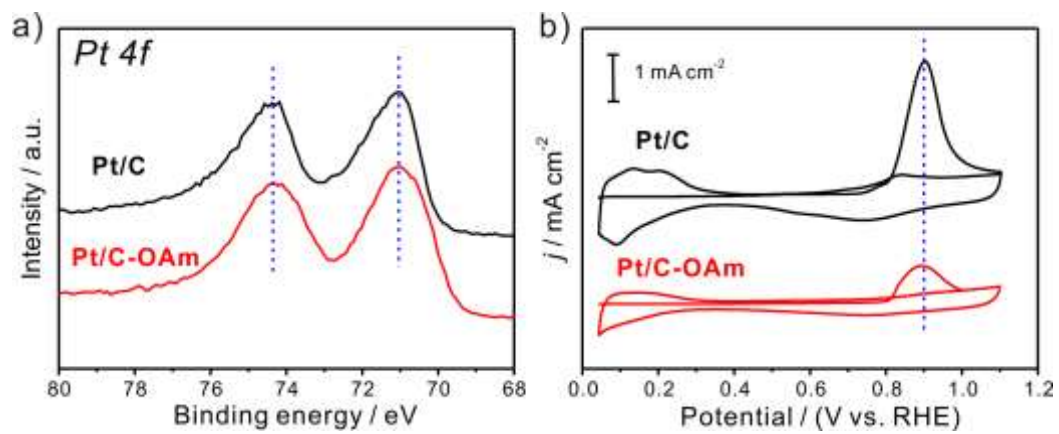


Fig. S17. XPS spectra (a) and CO stripping in 0.1 M HClO₄ (b) measurements of Pt/C and OAm modified Pt/C.

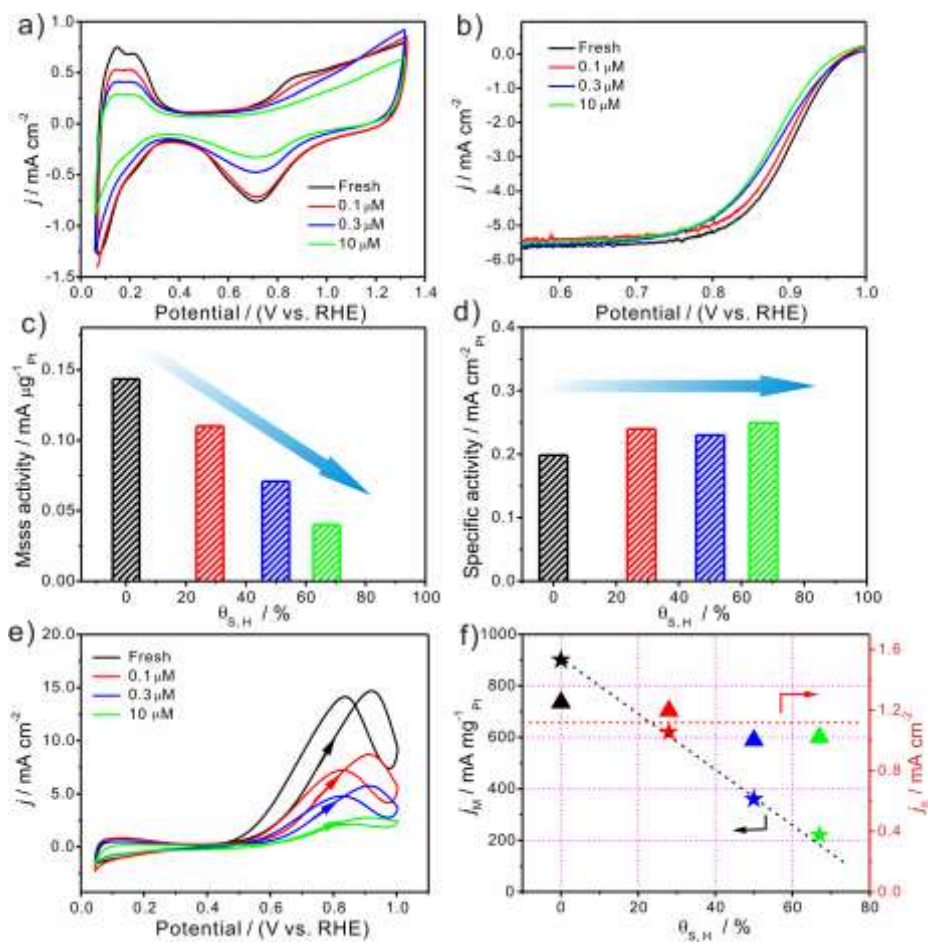


Fig. S18. The case of butylamine (BAm) ligand. (a) CVs operated in N_2 -saturated 0.1 M $HClO_4$ solution of Pt/C catalyst immersed in different concentrations of BAm/ethanol mixture. (b) LSV curves of Pt/C catalyst immersed in different concentrations of BAm/ethanol mixture. Mass activity (c) and specific activity (d) of Pt/C catalyst as a function of surface coverage of BAm derived from hydrogen desorption. (e) MOR curves in 0.1 M $HClO_4$ + 0.1 M CH_3OH solution of Pt/C and Pt/C with different surface coverages of BAm. (f) MOR mass activity (left) and specific activity (right) versus surface coverage of BAm on carbon supported Pt.

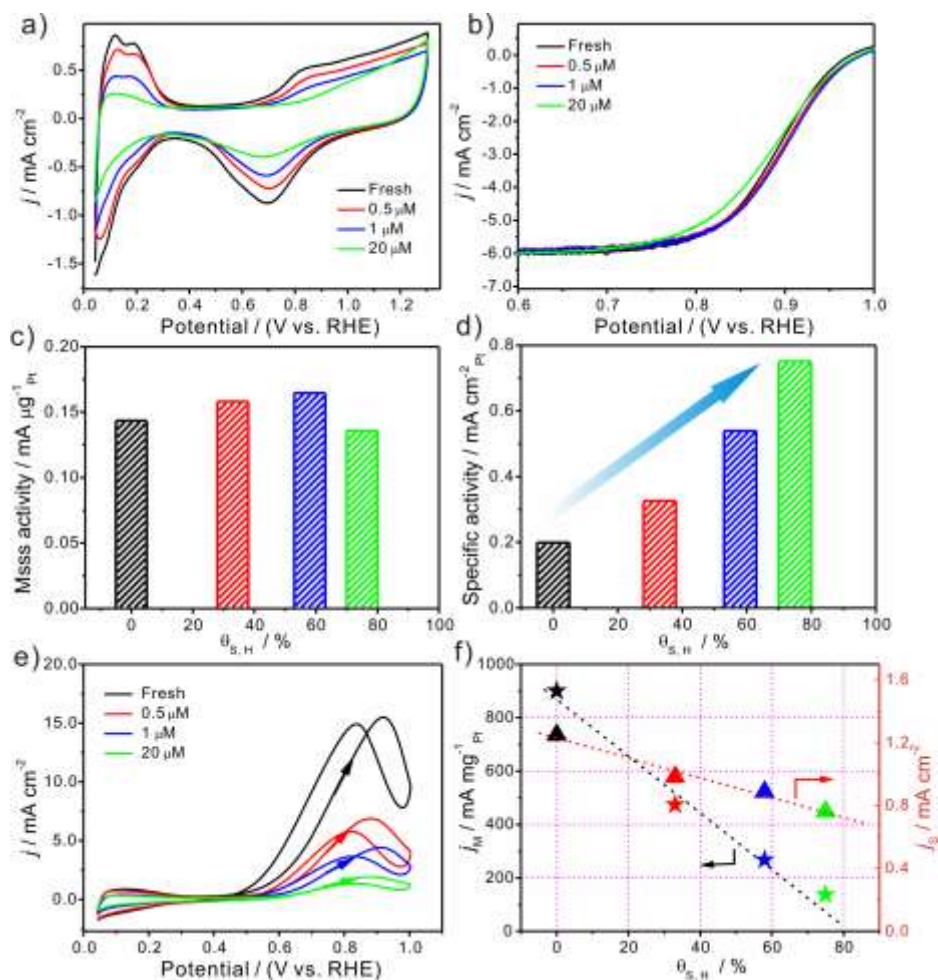


Fig. S19. The case of triphenylphosphine (TPP) ligand. (a) CVs operated in N_2 -saturated 0.1 M $HClO_4$ solution of Pt/C catalyst immersed in different concentrations of TPP/ethanol mixture. (b) LSV curves of Pt/C catalyst immersed in different concentrations of TPP/ethanol mixture. Mass activity (c) and specific activity (d) of Pt/C catalyst as a function of surface coverage of TPP derived from hydrogen desorption. (e) MOR curves in 0.1 M $HClO_4$ + 0.1 M CH_3OH solution of Pt/C and Pt/C with different surface coverages of TPP. (f) MOR mass activity (left) and specific activity (right) versus surface coverage of TPP on carbon supported Pt.

Supporting References:

1. P. J. Ferreira, Y. Shao-Horn, D. Morgan, R. Makharia, S. Kocha and H. A. Gasteiger, *J. Electrochem. Soc.*, 2005, **152**, 2256-2271.
2. J. Zhang, K. Sasaki, E. Sutter and R. R. Adzic, *Science*, 2007, **315**, 220-222.
3. T. V. Cleve, S. Moniri, G. Belok, K. L. More and S. Linic, *ACS Catal.*, 2016, **7**, 17-24.
4. S. Rudi, C. Cui, L. Gan and P. Strasser, *Electrocatalysis*, 2014, **5**, 408–418.
5. K. J. J. Mayrhofer, D. Strmcnik, B. B. Blizanac, V. Stamenkovic, M. Arenz and N. M. Markovic, *Electrochim. Acta*, 2008, **53**, 3181-3188.
6. D. F. van der Vliet, C. Wang, D. Li, A. P. Paulikas, J. Greeley, R. B. Rankin, D. Strmcnik, D. Tripkovic, N. M. Markovic and V. R. Stamenkovic, *Angew. Chem. Int. Ed.*, 2012, **51**, 3139-3142.
7. F. Somodi, I. Borbath, M. Hegedűs, A. Tompos, I. E. Sajo, A. Szegedi, S. Rojas, J. L. G. Fierro and J. L. Margitfalvi, *Appl. Catal. A: Gen.*, 2008, **347**, 216-222.
8. G. Kresse and J. Furthmüller, *Phys. Rev. B*, 1996, **54**, 11169-11186.
9. P. E. Blöchl, *Phys. Rev. B*, 1994, **50**, 17953-17979.
10. J. P. Perdew, K. Burke and M. Ernzerhof, *Phys. Rev. Lett.*, 1996, **77**, 3865-3868.
11. M. P. Teter, M. C. Payne and D. C. Allan, *Phys. Rev. B*, 1989, **40**, 12255-12263.
12. S. Grimme, J. Antony, S. Ehrlich, H. Krieg, *J. Chem. Phys.*, 2010, **132**, 154104.
13. S. Grimme, S. Ehrlich and L. Goerigk, *J. Comput. Chem.*, 2011, **32**, 1456-1465.
14. J. K. Nørskov, J. Rossmeisl, A. Logadottir, L. R. K. J. Lindqvist, J. R. Kitchin, T. Bligaard and H. Jonsson, *J. Phys. Chem. B*, 2004, **108**, 17886-17892.
15. L. Yu, X. Pan, X. Cao, P. Hu and X. Bao, *J. Catal.*, 2011, **282**, 183-190.
16. S. Kattel, P. Atanassov and B. Kiefer, *J. Phys. Chem. C*, 2012, **116**, 17378-17383.
17. K. Srinivasu and S. K. Ghosh, *J. Phys. Chem. C*, 2013, **117**, 26021-26028.
18. J. V. Lauritsen and F. Besenbacher, *Nova Acta Leopoldina*, 2005, **340**, 21-28.
19. J. Liu, M. Jiao, L. Lu, H. M. Barkholtz, Y. Li, Y. Wang, L. Jiang, Z. Wu, D. Liu, L. Zhuang, C. Ma, J. Zeng, B. Zhang, D. Su, P. Song, W. Xing, W. Xu, Y. Wang, Z. Jiang, G. Sun, *Nat. Commun.*, 2017, **8**, 15938.